J|A|C|S
ARTICLES
Published on Web 02/06/2004

Reactivity of Radicals Generated on Irradiation of *trans*-[Ru(NH$_3$)$_4$(NO$_2$)P(OEt)$_3$](PF$_6$)

Rose Maria Carlos,[†] Daniel Rodrigues Cardoso,[†] Eduardo Ernesto Castellano,[‡] Renata Zachi Osti,[†] Ademir João Camargo,[†] Luis Guilherme Macedo,[†] and Douglas Wagner Franco*,[‡]

Contribution from the Instituto de Química de São Carlos, IQSC-USP, Avenida Trabalhador SãoCarlense, 400, CP 780, CEP 13560-970, São Carlos - SP, Brazil, and Instituto de Física de São Carlos, IFSC-USP, Avenida Trabalhador SãoCarlense, 400, CP 369, CEP13566-590, São Carlos - SP, Brazil

Received July 16, 2003; E-mail: douglas@iqsc.usp.br

Abstract: The electronic absorption spectrum of *trans*-[Ru(NH$_3$)$_4$(NO$_2$)(P(OEt)$_3$]$^+$ in aqueous solution is characterized by a strong absorption band at 334 nm (λ_{max} = 1800 mol^{-1} L cm^{-1}). On the basis of quantum mechanics calculations, this band has been assigned to a MLCT transition from the metal to the nitro ligand. Molecular orbital calculations also predict an LF transition at 406 nm, which is obscured by the intense MLCT transition. When *trans*-[Ru(NH$_3$)$_4$(NO$_2$)(P(OEt)$_3$]$^+$ in acetonitrile is irradiated with a 355 nm pulsed laser light, the absorption features are gradually shifted to represent those of the solventocomplex *trans*-[Ru(NH$_3$)$_4$(solv)(P(OEt)$_3$]$^{2+}$ (λ_{max} = 316 nm, ϵ = 650 mol^{-1} L cm^{-1}), which was also detected by ^{31}P NMR spectroscopy. The net photoreaction under these conditions is a photoaquation of *trans*-[Ru(NH$_3$)$_4$(NO$_2$)(P(OEt)$_3$]$^+$, although, after photolysis, the presence of the nitric oxide was detected by differential pulse polarography. In phosphate buffer pH 9.0, after 15 min of photolysis, a thermal reaction resulted in the formation of a hydroxyl radical and a small amount of a paramagnetic species as detected by EPR spectroscopy. In the presence of *trans*-[Ru(NH$_3$)$_4$(solv)P(OEt)$_3$]$^{2+}$, the hydroxyl radical initiated a chain reaction. On the basis of spectroscopic and electrochemical data, the role of the radicals produced is analyzed and a reaction sequence consistent with the experimental results is proposed. The 355 nm laser photolysis of *trans*-[Ru(NH$_3$)$_4$(NO$_2$)(P(OEt)$_3$]$^+$ in phosphate buffer pH 7.4 also gives nitric oxide, which is readily trapped by ferrihemeproteins (myoglobin, hemoglobin, and cytochrome C), giving rise to the formation of their nitrosylhemeproteins(II), (NO)Fe(II)hem.

Introduction

Nitric oxide is widely recognized as a biologically important molecule, regulating blood pressure, acting as a neurotransmitter, and participating in the ability of the immune system to kill tumor cells and intracellular parasites.[1−5] Regarding the photochemical behavior of nitric oxide, coordination complexes of iron, cobalt, chromium, and ruthenium with nitrosyl groups have been investigated to develop molecular devices for the delivery of nitric oxide and targeting processes.[6−9] In this respect, our laboratory is interested in studying ruthenium(II) ammine complexes that may serve as potential photochemical precursors of nitric oxide.[10−15] Previous studies have demonstrated the photolability of *trans*-[Ru(NH$_3$)$_4$(NO)L]$^{3+}$ complexes thereby releasing nitric oxide in aqueous solution.[15] These complexes exhibit desirable qualities such as water solubility, stability, and toxicity[10−12,15] for the delivery of nitric oxide to biological targets, while quantum yields are elevated (0.1−0.3 mol einstein^{-1}). However, their absorptivities are relatively low (200−600 mol^{-1} L cm^{-1}). To increase the scope of ruthenium complexes, *trans*-[Ru(NH$_3$)$_4$(NO$_2$)P(OEt)$_3$]$^+$ has been synthesized, for which the ligand field is weaker than that for the nitrosyl containing the complex. Furthermore, the *trans*-[Ru(NH$_3$)$_4$(NO$_2$)P(OEt)$_3$]$^+$ complex exhibits an intense charge-transfer transition ($\epsilon \approx$ 1800

[†] IQSC-USP.
[‡] IFSC-USP.

(1) Wang, P. G.; Xian, M.; Tang, M. X.; Wu, X.; Wen, Z.; Cai, T.; Janczuk, A. J. *Chem. Rev.* **2002**, *102*, 1091−1134.
(2) Feelish, M., Stamler, J. S., Eds. *Methods in Nitric Oxide Research*; Wiley: Chichester, U.K., 1996.
(3) Cooper, C. E. *Biochim. Biophys. Acta* **1999**, *290*, 1411−1418.
(4) Ford, P. C.; Bourassa, J.; Miranda, K.; Lee, B.; Lorkovic, I.; Boggs, S.; Kudo, S.; Laverman, L. *Coord. Chem. Rev.* **1998**, *171*, 185−202.
(5) Stochel, G.; Wanat, A.; Kulis, E.; Stasicka, Z. *Coord. Chem. Rev.* **1998**, *171*, 203−220.
(6) DeLeo, M. A.; Ford, P. C. *Coord. Chem. Rev.* **2000**, *208*, 47−62.
(7) Cheng, L.; Movozhilova, I.; Kim, C.; Kovalevsky, A.; Bagley, K. A.; Coppens, P.; Richter-Addo, G. B. *J. Am. Chem. Soc.* **2000**, *122*, 7142−7143.
(8) Works, C. F.; Jocher, C. J.; Bart, G. D.; Bu, X.; Ford, P. C. *Inorg. Chem.* **2002**, *41*, 3728−3739.
(9) Bohle, D. S.; Hung, C. H.; Smith, B. D. *Inorg. Chem.* **1998**, *37*, 5798−5806.
(10) Wieraszko, A.; Clarke, M. J.; Lang, D. R.; Lopes, L. G. F.; Franco, D. W. *Life Sci.* **2001**, *68*, 1535−1540.
(11) Torsoni, A. S.; Barros, B. F.; Toledo, J. C.; Haun, M.; Krieger, M. H.; Tfouni, E.; Franco, D. W. *Life Sci.* **2001**, *68*, 1535−1540.
(12) Borges, S. S. S.; Davanzo, C. U.; Z-Schpcetor, J.; Castellano, E. E.; Silva, S. C.; Franco, D. W. *Inorg. Chem.* **1998**, *37*, 2670−2677.
(13) Gomes, M. G.; Davanzo, C. U.; Silva, S. C.; Lopes, L. G. F.; Santos, P. S.; Franco, D. W. *J. Chem. Soc., Dalton Trans.* **1998**, 601−607.
(14) Gorelsky, S. I.; Silva, S. C.; Lever, A. B. P.; Franco, D. W. *Inorg. Chim. Acta* **2000**, *300*, 698−708.
(15) Tfouni, E.; Krieger, M.; McGarvey, B. R.; Franco, D. W. *Coord. Chem. Rev.* **2003**, *236*, 57−69.

10.1021/ja0373263 CCC: $27.50

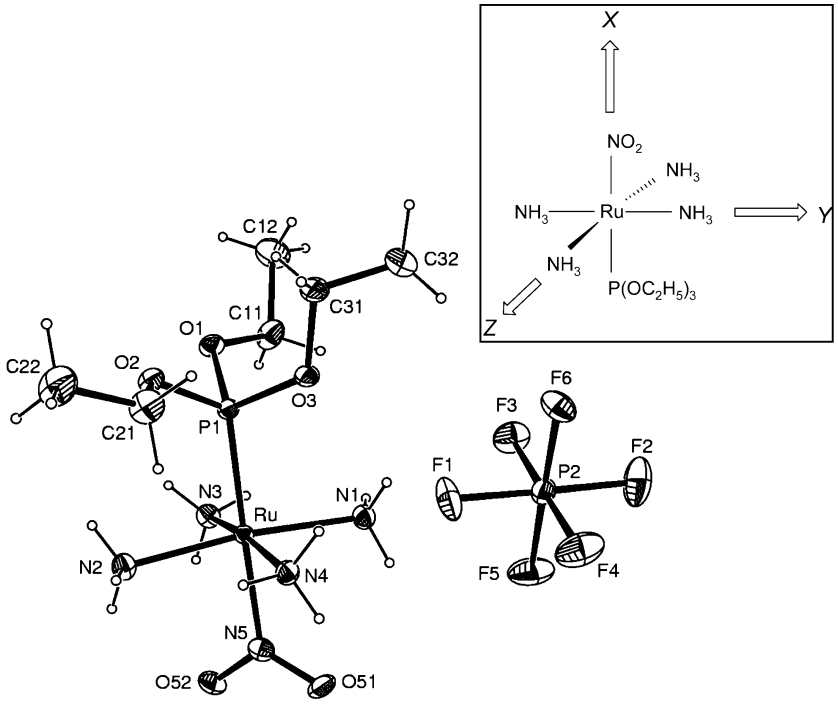

Figure 1. A view from the DFT calculation of the coordinated geometry of *trans*-$[Ru(NH_3)_4(NO_2)P(OEt)_3]^+$. Inset: Orientation of the axis adopted by the DFT calculation.

mol^{-1} L cm^{-1}) in the 330 nm region. The present paper describes the X-ray data, molecular orbital calculations, UV−vis spectral data, and photochemical properties of *trans*-$[Ru(NH_3)_4(NO_2)P(OEt)_3]^+$ in both aqueous phosphate buffer and acetonitrile. The thermal and photochemical reactions of *trans*-$[Ru(NH_3)_4(NO_2)(P(OEt)_3]^+$, in phosphate pH 7.4 containing hemeproteins (myoglobin(III), hemoglobin(III), and cytochrome C), are also presented.

Experimental Section

Materials. Analytical-grade chemicals and HPLC grade solvents were used for all experiments. Acetonitrile was stored over molecular sieves. Oxidized forms of hemoglobin (human), myoglobin (horse heart), and cytochrome C (horse heart) were obtained from Sigma and used as supplied. The pH values (pH 7−8) of phosphate buffer (ionic strength, 0.2) were adjusted with the use of aqueous solutions of 0.025 mol L^{-1} KH_2PO_4 and 0.025 mol L^{-1} K_2HPO_4. At a pH higher than 8.0, 0.05 mol L^{-1} Na_2BO_4 buffer was used.

trans-$[Ru(NH_3)_4(H_2O)P(OEt)_3](PF_6)_2$ was obtained as a white solid following the literature procedure.[16,17] *trans*-$[Ru(NH_3)_4(NO_2)P(OEt)_3](PF_6)$ was synthesized by the reaction of 200 mg of *trans*-$[Ru(NH_3)_4(H_2O)P(OEt)_3]^{2+}$ and 250 mg of $NaNO_2$ in 2 mL of degassed Milli-Q water at room temperature. After 30 min of reaction, 200 mg of NH_4PF_6 was added, and the yellow solution was kept in the refrigerator for 12 h. *trans*-$[Ru(NH_3)_4(NO_2)P(OEt)_3](PF_6)$ was collected by filtration, washed with diethyl ether, and dried under vacuum. The yield was ca. 65%. The solid complex was stable for several days when stored in the dark under inert atmosphere. Anal. Calcd: Ru, 19.2; C, 13.7; N, 13.3; H, 5.2. Found: Ru, 18.5; C, 14.0; N, 13.9; H, 5.3. IR data: 1633 cm^{-1} (w), δ NH_3; 1400 cm^{-1} (s), ν_a NO_2; 1024 cm^{-1} (s), δ P−O−C; 834 cm^{-1} (s) ν PF_6; and 560 cm^{-1} (s) δ PF_6.

trans-$[Ru(NH_3)_4(H_2O)P(OEt)_3](PF_6)_3$ was generated by electrolysis of the corresponding Ru(II) complex.[18] In a typical experiment, a sample of ca. 200 mg of *trans*-$[Ru(NH_3)_4(H_2O)P(OEt)_3](PF_6)_2$ was dissolved in 40 mL of degassed CF_3COOH (pH 2.0). Exhaustive electrolysis at +0.70 V vs SCE using the Pt plate as working and counter electrodes and an Ag wire coated by AgCl in a capillary as the reference electrode provided *trans*-$[Ru(NH_3)_4(H_2O)P(OEt)_3]^{3+}$. When the oxidation was complete, the solvent was removed, and the residue was washed with ethanol and ether.

Crystal Data and Data Collection. Crystals of $C_6H_{27}F_6N_5O_5P_2Ru$ were obtained from an aqueous solution maintained in the refrigerator for 4 days, under argon atmosphere. A yellow crystal fragment (0.10 mm × 0.12 mm × 0.12 mm) of the complex was used in the single-crystal X-ray diffraction experiment. All measurements were taken in an Enraf-Nonius Kappa CCD diffractometer with graphite monochromated Mo Kα (λ = 0.71073 Å) radiation. $C_6H_{27}F_6N_5O_5P_2Ru$, FW = 526.34, T = 120(2) K, λ = 0.71073 Å, orthorhombic, space group $P2_12_12_1$, a = 10.134(1) Å, b = 10.200(1) Å, c = 19.395(1) Å, V = 2004.80(8) $Å^3$, Z = 4, ρ = 1.744 Mg $(m^3)^{-1}$, μ = 1.021 mm^{-1}, F(000) = 1064. Data collection range 2.91−26.0°, $-12 \le h \le 11$, $-12 \le k \le 12$, $-23 \le l \le 23$. Reflections collected/unique 11 811/3860 (R(int) = 0.049).

Structure Solution and Refinement. The structure was solved by direct methods with *SHELXS-97*.[19] The Fourier map obtained showed all non-hydrogen atoms. The model was refined by full-matrix least-squares procedure on F^2 by means of *SHELXL-97*.[19] The hydrogen atoms of the CH_2 groups were set isotropic with a thermal parameter 20% greater than the equivalent isotropic displacement parameter of the carbon atom to which each one is bonded; this percentage was set to 50% for the hydrogen atoms of the NH_3 and CH_3 groups. All of the hydrogen atoms were stereochemically positioned and refined with the riding model.[19] Final R indices [3771 reflections with $I > 2\sigma(I)$] = R1 = 0.0246, wR2 = 0.0606, R indices (all data) R1 = 0.0256, wR2 = 0.0612. Absolute structure parameter −0.01 (2). Largest difference peak and hole 0.357 and −0.656 e $Å^{-3}$. An ORTEP[20,21] projection of the complex is shown in Figure 1.

(16) Franco, D. W.; Taube, H. *Inorg. Chem.* **1978**, *17*, 571−578.
(17) Rezende, N. M. S.; Martins, S. C.; Marinho, L. A.; Santos, J. A. V.; Tabak, M.; Perussi, J. R.; Franco, D. W. *Inorg. Chim. Acta* **1991**, *182*, 87−92.
(18) Mazzeto, S. E.; Rodrigues, E.; Franco, D. W. *Polyhedron* **1993**, *12*, 971−975.
(19) Sheldrick, G. M. *SHELX97, Programs for Crystal Structure Analysis (Release 97-2)*; Institüt für Anorganische Chemie der Universität: Tammanstrasse 4, D-3400 Göttingen, Germany, 1998.

Electrochemical NO Detection. The release of NO in CH_3CN was monitored using an EG&G Princeton Applied Research model 264A polarographic analyzer/stripping voltammeter in conjunction with a three electrode cell. Differential pulse voltammograms were obtained in CH_3CN at 22 °C in a voltammetric cell with a glassy-carbon electrode as the working electrode, a platinum wire as the auxiliary, and an SCE reference electrode. Nitric oxide quantitative measurements were performed using an NO sensor electrode from Innovative Instruments, Inc., a model amiNO700 electrode with an *in*NO Nitric Oxide Measuring System.

Photochemistry. The complex was irradiated using the third harmonic (355 nm) of an Nd:YAG 10 ns pulse width laser (Continuum Surelite OPO IIP-10) attenuated to approximately 2 mJ/pulse as the excitation source. The progress of the photoreaction was monitored spectrophotometrically in a Hitachi model U2000 spectrophotometer. The photolysis was performed at 25 °C in 1.0 cm path length quartz cells capped with a rubber septum. The solutions ($10^{-3}-10^{-4}$ mol L^{-1} initial complex concentration) were deaerated by bubbling with argon prior to photolysis and were stirred during irradiation. The solutions were photolyzed to approximately 10% conversion. Dark reactions were performed simultaneously using solutions of identical composition. As analyzed from their UV−vis spectra, these samples were stable in the dark in a time scale longer than that of the photochemical experiments. Photoproducts were identified by comparing their UV−vis spectra with the spectra of solvent-substituted ruthenium(II) phosphite complex[16,17] *trans*-$[Ru(NH_3)_4(H_2O)P(OEt)_3]^{2+}$. Compounds formed by dark reactions were identified by NMR, EPR, and electrochemical (differential pulse voltammetry and electrolysis) techniques.

^{31}P NMR spectra were obtained using 5 mm vacuum NMR tubes (Wilmad) in a Bruker DRX 400 9.4 T (161.9 MHz to ^{31}P) spectrometer. The sample (ca. 30 mg) was dissolved in the appropriate solvent, and D_2O served as a reference. The dearation of solutions was achieved with 3−5 vacuum−argon cycles in a Schlenk line.

EPR measurements were taken using a quartz flat cell at room temperature or 2 mm quartz tubes for 77 K (Wilmad) in a Bruker ESP 300E X-band spectrometer equipped with a TE102 standard cavity. The experiment at 77 K was performed using a quartz Dewar filled with liquid nitrogen.

Heme Proteins Nitrosylation. All of the sample solutions were prepared in the vacuum line with meticulous care to avoid oxygen contamination. A glass apparatus used for the present study consists of a round-bottomed vessel (2 mL) connected to a quartz cell (1 cm optical path length) fixed to a gas/vacuum manifold by a glass joint. After the phosphate buffer (pH 7.4) solution of *trans*-$[Ru(NH_3)_4(NO_2)P(OEt)_3]^+$ was degassed, the hemeprotein (hem) was introduced into the round-bottom vessel, and the system was deaerated with four vacuum−argon cycles. The absorption spectrum of the aqueous solutions of the complex was measured and photolyzed with 355 nm light for 6 min. When the irradiation was stopped, the hem was mixed, and the subsequent thermal reaction was followed by changes in the UV−vis absorption spectrum of the protein. Products were identified by comparing their UV−vis spectra with the spectra of the $(NO)Fe^{II/III}$ hem adduct.[22,23] The absorption spectrum of hem in the presence of the complex was stable in the dark for long periods.

Computational Details. All calculations were performed using the Gaussian 98 suite of programs.[24] The starting molecular geometries were obtained at the UHF/3-21G level of theory. The final molecular geometry optimizations were performed using the Kohn−Sham density functional theory (DFT) with the Becke three-parameters hybrid exchange-correlation functional[24] known as B3LYP at the 6-31(d) level of theory for H, C, N, O, and P, and 3-21 g(d) with LanL2DZ pseudo potential[25] for Ru. The analytical evaluation of the energy second derivative matrix in Cartesian coordinates (Hessian matrix) at the same level of approximation confirmed the nature of minima of the potential surface points associated with the optimized structures.

Time-dependent density functional theory[26−28] (TD-DFT) allowed the computation of excitation energies, oscillator strengths, and composition determinants. TD-DFT calculations were performed using the B3LYP hybrid functional and the 6-31++G(d,p) basis set for H, C, N, O, and P, and an effective core potential LanL2DZ for Ru. The excited state compositions were described as a linear combination of singly excited Slater determinants; their relative weights are represented by the normalized squared coefficients in the linear combination.

Table 1. Selected Bond Lengths (Å) and Angles (deg)

atoms	dist	atoms	angle
Ru−N5	2.096(3)	N5−Ru−P1	178.47(7)
Ru−N4	2.141(2)	N4−Ru−P1	93.08(7)
Ru−N2	2.133(2)	N2−Ru−P1	94.01(7)
Ru−N3	2.141(2)	N3−Ru−P1	95.01(7)
Ru−N1	2.142(2)	N1−Ru−P1	92.39(7)
Ru−P1	2.217(1)	O51−N5−O52	117.7(2)
P1−O2	1.615(2)	O51−N5−Ru	120.9(2)
P1−O1	1.614(2)	O52−N5−Ru	121.4(2)
P1−O3	1.604(2)		
O1−C11	1.452(4)		
O2−C21	1.451(3)		
O51−N5	1.251(3)		
O3−C31	1.462(4)		

Results and Discussion

Molecular Structure. Table 1 shows the selected interatomic distances. The mean $Ru-NH_3$ distance is determined as 2.14(4) Å, which is in agreement with that (2.13 ± 0.01 Å) in *trans*-$[Ru(NH_3)_5NO_2]Cl$[29] and that (2.10 ± 0.06 Å) in *trans*-$[Ru(NH_3)_4(NO)(nic)](SiF_6)_3 \cdot 2H_2O$.[12] The Ru−P distance [2.2171(8) Å] is shorter than that (2.366 Å) in *trans*-$[Ru(NH_3)_4(P(OEt)_3)_2](PF_6)_2$.[16] The $P-Ru-N(NO_2)$ bond angle is 178.47(7)°, indicating that the $P-Ru-N(NO_2)$ bond is almost linear. The O−N−O angle of the NO_2 in the moiety *trans*-$[Ru(NH_3)_4(NO_2)P(OEt)_3](PF_6)$ is 117.7(2)°, similar to those obtained for $[Ru(NO_2)(PMe_3)_3(trpy)](ClO_4)$ (114.8°), *trans*-$[Ru(NH_3)_5NO_2]Cl$ (113.2°), and $[Ru(trpy)(NC_5H_4N{=}NC_6H_4(8\text{-}Me))NO_2]ClO_4 \cdot C_6H_6$ (117.6°).[29,30]

Molecular Orbital Results. For DFT calculations, the $(P(OEt)_3)P-Ru-N(NO_2)$ vector is defined as *x*, while *z* and *y* lie close to the $Ru-NH_3$ vectors (Figure 1, inset).

(20) Sheldrick, G. M. *SHELX93, Program for Crystal Structure Determination*; University of Gottingen: Gottingen, Germany, 1993.
(21) Johson, C. K. ORTEPII Report ORNL-5138; Oak Ridge National Laboratory: Oak Ridge, TN, 1976.
(22) Hoshino, M.; Ozawa, K.; Seki, H.; Ford, P. C. *J. Am. Chem. Soc.* **1993**, *115*, 9568−9575.
(23) Hoshino, M.; Maeda, M.; Konishi, R.; Seki, H.; Ford, P. C. *J. Am. Chem. Soc.* **1996**, *118*, 5702−5707.
(24) Frisch, M. J.; Trucks, G. W.; Schlegel, H. B.; Scuseria, G. E.; Robb, M. A.; Cheeseman, J. R.; Zakrzewski, V. G.; Montgomery, J. A., Jr.; Stratmann, R. E.; Burant, J. C.; Dapprich, S.; Millam, J. M.; Daniels, A. D.; Kudin, K. N.; Strain, M. C.; Farkas, O.; Tomasi, J.; Barone, V.; Cossi, M.; Cammi, R.; Mennucci, B.; Pomelli, C.; Adamo, C.; Clifford, S.; Ochterski, J.; Petersson, G. A.; Ayala, P. Y.; Cui, Q.; Morokuma, K.; Malick, D. K.; Rabuck, A. D.; Raghavachari, K.; Foresman, J. B.; Cioslowski, J.; Ortiz, J. V.; Stefanov, B. B.; Liu, G.; Liashenko, A.; Piskorz, P.; Komaromi, I.; Gomperts, R.; Martin, R. L.; Fox, D. J.; Keith, T.; Al-Laham, M. A.; Peng, C. Y.; Nanayakkara, A.; Gonzalez, C.; Challacombe, M.; Gill, P. M. W.; Johnson, B. G.; Chen, W.; Wong, M. W.; Andres, J. L.; Head-Gordon, M.; Replogle, E. S.; Pople, J. A. *Gaussian 98*, revision A.6; Gaussian, Inc.: Pittsburgh, PA, 1998.
(25) Wadt, W. R.; Hay, P. J. *J. Chem. Phys.* **1985**, *82*, 284−298.
(26) Becke, A. D. *J. Chem. Phys.* **1993**, *98*, 5648−5652.
(27) Casida, M., Chong, D. P., Eds. *Recent Advances in Density Functional Methods*; World Scientific: Singapore, 1995; Vol. 1, p 155.
(28) Casida, M. E.; Jamorski, K. C.; Casida, D. R.; Salahub, D. R. *J. Chem. Phys.* **1998**, *108*, 4439−4449.
(29) Bottomley, F. *J. Chem. Soc., Dalton Trans.* **1972**, 2148−2152.
(30) Leising, R. A.; Kubow, S. A.; Churchill, M. R.; Buttrey, L. A.; Ziller, J. W.; Takeuchi, K. J. *Inorg. Chem.* **1990**, *29*, 1306−1312.

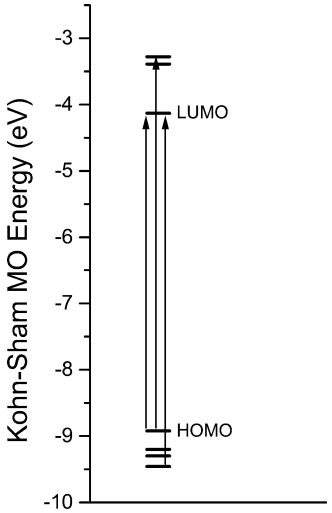

Figure 2. Relevant parts of the molecular orbital diagram of *trans*-[$Ru(NH_3)_4(NO_2)P(OEt)_3]^+$.

The quantum chemical calculations gave distances for Ru−N(NH_3) of 2.20 Å, Ru−N(NO_2) of 2.06 Å, and Ru−P($P(OEt)_3$) of 2.31 Å, in very good agreement with those obtained from single-crystal X-ray data. The calculated N−O distances from NO_2^- are 1.24 Å. The complex has C_1 symmetry with P, Ru, and N (all on the *x* axis) of the axial nitro ligand in the same plane of symmetry. The NO_2^- group lies on a plane parallel to the *x* axis and bisects the *y* and *z* axes, that is, the NH_3 axes.

Molecular Orbital Analysis. The frontier orbitals were obtained using the B3LYP functional. The HOMO has predominantly (60%) nonbonding d_{yz} character, while HOMO−1 has a nonbonding character with main contributions of (42%) d_{xy} and (23%) d_{xz}. The LUMO has 72% of NO_2 π^* character (p_z orbitals of N and both O). Interestingly, because the molecule belongs to the C_1 group, the LUMO+1 and LUMO+2 MOs have s, p_x, p_y, p_z, d_{z2}, and d_{x2-y2} contributions. The relative energies for HOMO and LUMO are −8.92 and −4.13 eV, respectively. It is important to notice that density functional methods usually give small HOMO−LUMO gaps. The next two empty MOs LUMO+1 and LUMO+2 are 0.74 and 0.85 eV higher in energy as compared to the LUMO energy. The HOMO−1 and HOMO−2 MOs are 0.28 and 0.38 eV below the HOMO energy. Because the energy difference between LUMO+1 and LUMO+2 is near 0.1 eV, the two states may be considered as nearly degenerated, which is also valid for HOMO−1 and HOMO−2 MOs. The MO diagrams of *trans*-$[Ru(NH_3)_4(NO_2)P(OEt)_3]^+$ are presented in Figure 2.

Electronic Spectrum. Figure 3 clearly shows that the nature of the solvent has a great influence on the position and the relative intensities of the absorption band of *trans*-$[Ru(NH_3)_4(NO_2)P(OEt)_3]^+$. In CH_3CN, the absorption spectrum shows a weak shoulder at about 290 nm and a band maximum at 308 nm. Changing the solvent from CH_3CN to phosphate buffer, pH = 9.7, results in a shift of the absoption maxima to longer wavelengths. At the same time, the intensity of the higher-lying absorption band increases with respect to that of the band of the lower one. On the basis of these effects, the bands are assigned as MLCT charge-transfer transitions from the metal to the nitro ligand. Indeed, these two close absorptions might belong to MLCT transitions from different metal-dπ orbitals to the lowest π^* orbital of the nitro ligand. This conclusion is in agreement with the results from the MO calculations. The lowest energy band, 3.66 eV (339 nm), is very likely a charge-transfer transition from the HOMO localized in the metal to the LUMO orbital localized in the nitro ligand. The second MLCT transition was calculated at 3.74 eV (331 nm) representing mainly a HOMO−3 to LUMO transition. The second transition is weaker, because the magnitude of its transition electric dipole moment is smaller (5.37×10^{-2} au) as compared to the former one (6.15×10^{-2} au).

The excited singlet state corresponding to a HOMO−LUMO excitation is calculated to be at 3.66 eV above the ground state, which is in remarkable agreement with the experimental energy of 3.71 eV.

Apart from the CT transitions, the nitro complex also possesses LF transitions at lower energies, as their low intensities are obscured by the intense CT transitions. In the MO diagrams of *trans*-$[Ru(NH_3)_4(NO_2)P(OEt)_3]^+$, the transitions from HOMO to LUMO+2 (11% p_y Ru, 9% p_z Ru, 21% d_{z2} Ru, 8% d_{x2-y2} Ru) with an energy of 3.05 eV (406 nm) can be considered to be LF transitions.

Photochemistry. The photolysis of *trans*-$[Ru(NH_3)_4(NO_2)P(OEt)_3]^+$ (6×10^{-4} mol L^{-1}) in CH_3CN with 355 nm light led to a progressive depletion of the characteristic absorption band at 308 nm (Figure 4) concomitantly with a blue shift to 292 nm. This new band profile is similar to that exhibited[17] by *trans*-$[Ru(NH_3)_4(H_2O)P(OEt)_3]^{2+}$ (λ_{max}= 292 nm, $\epsilon = \sim 8 \times 10^2$ mol^{-1} L cm^{-1}) in CH_3CN. Isosbestic points were observed, indicating that there is no spectrally significant buildup of intermediates and any potential secondary photolysis does not lead to measurable spectral changes. This observation was confirmed by the direct photolysis of the *trans*-aquophosphite species synthesized thermally.[16] No spectral changes were found after a long photolysis period of *trans*-$[Ru(NH_3)_4(H_2O)P(OEt)_3]^{2+}$ in CH_3CN.

The presence of *trans*-$[Ru(NH_3)_4(H_2O)P(OEt)_3]^{2+}$ in the photolyzed solution was confirmed through ^{31}P NMR measurements. The irradiation of *trans*-$[Ru(NH_3)_4(NO_2)P(OEt)_3]^+$ in CH_3CN for 30 min at room temperature afforded a well-resolved ^{31}P NMR spectrum with one signal at 147 ppm, which was assigned to *trans*-$[Ru(NH_3)_4(H_2O)P(OEt)_3]^{2+}$ (Figure 5).

Nitric oxide was detected in the analysis of partially photolyzed solutions (10−40% conversion) through differential pulse polarography (DPP), Figure 6. The anodic pulse observed at 0.80 V vs SCE was assigned to the oxidation of the radical produced. This peak was absent in solutions of *trans*-$[Ru(NH_3)_4(NO_2)P(OEt)_3]^+$ kept in the dark. The quantification of nitric oxide was performed using the NO sensor electrode. In such photolysis experiments, the NO concentration was determined electrochemically after ~20 min of photolysis of the *trans*-$[Ru(NH_3)_4(NO_2)P(OEt)_3]^+$ ($\sim 6.39 \times 10^{-4}$ mol L^{-1}) in CH_3CN. The data collected indicated that 100 nmol L^{-1} of NO was released per mol of photo converted complex.

It was possible to infer that the presence of nitric oxide was the result of the secondary photolysis of free nitrite. Additional support was provided by a photochemical study[31] which showed that the photolysis of the nitrite in aqueous solution in the 200−400 nm region leads to the production of both a nitrosyl radical

(31) Mack, J.; Bolton, J. R. *J. Photochem. Photobiol., A: Chem.* **1999**, 128, 1−13.

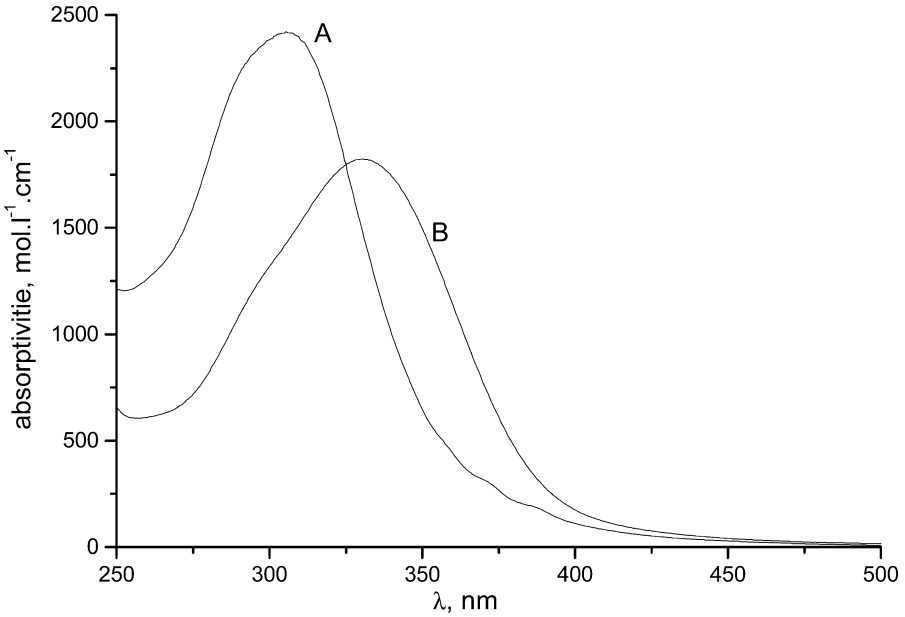

Figure 3. Absorption spectra of *trans*-$[Ru(NH_3)_4(NO_2)P(OEt)_3]^+$ in both CH_3CN (A) and phosphate buffer pH 9.3 (B).

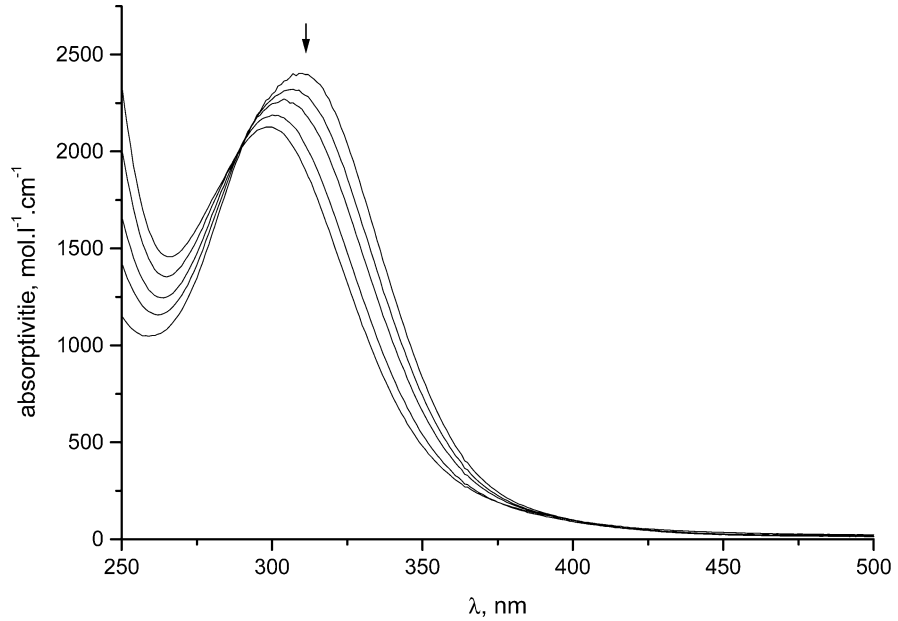

Figure 4. Spectral changes accompanying the photolysis of *trans*-$[Ru(NH_3)_4(NO_2)P(OEt)_3]^+$ in CH_3CN, $\lambda_{irr} = 355$ nm.

and an oxygen radical anion. The recombination is likely to occur due to the high reactivity of the species.[31−33] The observance of nitric oxide suggests that where aprotic solvents are present the oxygen radical anion is trapped, probably by the solvent, allowing for the observation of NO. Therefore, the observation of *trans*-$[Ru(NH_3)_4(H_2O)P(OEt)_3]^{2+}$ as the primary photolysis product in CH_3CN would be consistent with the reaction Scheme 1.

The spectral changes were totally different when *trans*-$[Ru(NH_3)_4(NO_2)P(OEt)_3]^+$ was photolyzed in phosphate buffer pH 9.0. The irradiation at 355 nm of a solution containing $\sim 7 \times 10^{-4}$ mol L^{-1} complex led to spectral variations, which were in accordance with those found in CH_3CN for a time period corresponding to about 25% conversing, that is, a continuous decrease in the absorbance around 330 nm and a shift in the maximum absorption to 316 nm (Figure 7). However, when the irradiation was stopped and the sample was allowed to remain in the dark for 20 min, a final spectrum was observed, which was similar to that of *trans*-$[Ru(NH_3)_4(H_2O)P(OEt)_3]^{3+}$ in the same solvent ($\lambda_{max} = 285$ nm, $\epsilon \approx 800$ mol^{-1} L cm^{-1}). The analysis was based on the changes in a photolyzed solution of *trans*-$[Ru(NH_3)_4(NO_2)P(OEt)_3]^+$ using ^{31}P NMR spectroscopy. The spectral changes (Figure 8) indicate that the disappearance of the *trans*-$[Ru(NH_3)_4(NO_2)P(OEt)_3]^+$ signal is accompanied by the appearance of a new signal at 147 ppm characteristic of ^{31}P in *trans*-$[Ru(NH_3)_4(H_2O)P(OEt)_3]^{2+}$, as well as of an unidentified species with a ^{31}P signal at 143 ppm. A signal for a free phosphite ligand was also observed at 9 ppm.

The presence of a paramagnetic ruthenium species was detected in the EPR spectra of photolyzed *trans*-$[Ru(NH_3)_4$-

(32) Meyrstein, D. *Acc. Chem. Res.* **1978**, *11*, 43−48.
(33) Stanbury, D. M. *Adv. Inorg. Chem.* **1989**, *33*, 69−80.

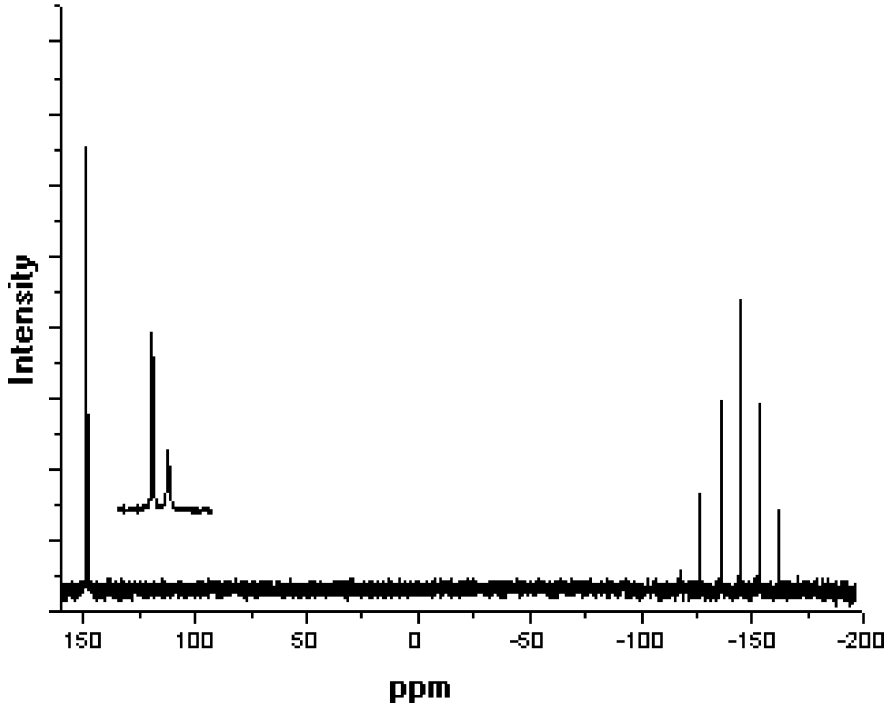

Figure 5. ^{31}P NMR spectrum of *trans*-$[Ru(NH_3)_4(NO_2)P(OEt)_3]^+$ in CH_3CN after 30 min of photolysis.

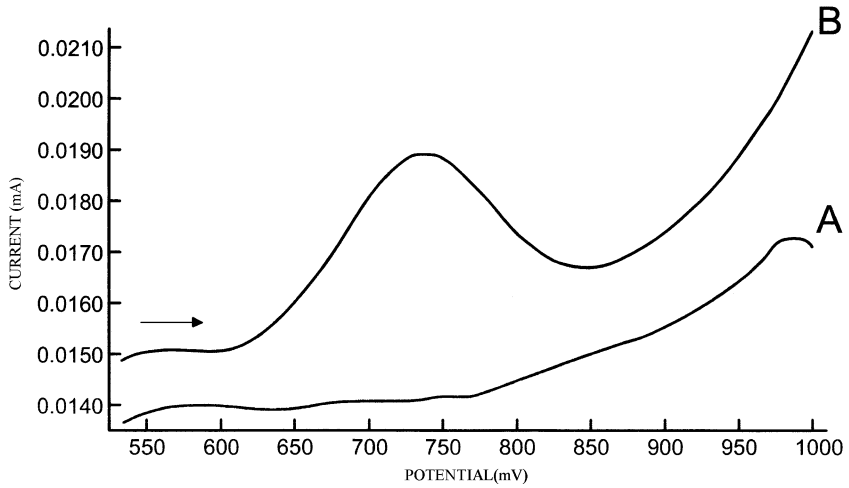

Figure 6. Differential pulse voltammogram of *trans*-$[Ru(NH_3)_4(NO_2)P(OEt)_3]^+$ complex in CH_3CN at the glassy-carbon electrode with platinum wire as an auxiliary electrode and SCE as the reference electrode. (A) Before photolysis, (B) after photolysis.

Scheme 1. Primary Step during the 355 nm Photolysis of *trans*-$[Ru(NH_3)_4(NO_2)P(OEt)_3]^+$

$$\textit{trans}\text{-}[Ru(NH_3)_4(NO_2)P(OEt)_3]^+ \xrightarrow{h\nu} \textit{trans}\text{-}[Ru(NH_3)_4(H_2O)P(OEt)_3]^{2+} + (NO_2)^-$$

$$(NO_2)^- \xrightarrow{h\nu} NO^\bullet + O^{\bullet-}$$

$(NO_2)P(OEt)_3]^+$ solutions. The (frozen solution) EPR spectrum observed ca. 20 min after irradiation shows a small amount of an unidentified species at $g = 2.06$, which is neither stable nor frequently evident during the experiments (Figure 9). This observation would suggest that, in the decay processes, the autoxidation or diffusion from the solution may be occurring.

As previously reported, the stability of *trans*-$[Ru(NH_3)_4(H_2O)P(OEt)_3]^{3+}$ is highly pH-dependent.[17,18] At pH > 11, a disproportionate reaction is suggested to occur, yielding Ru(II) and Ru(VI) as the major entities.[18] It is also argued that, in alkaline solutions, Ru(II) and Ru(VI) are expected to be more stable than Ru(III). The EPR spectrum of *trans*-$[Ru(NH_3)_4(H_2O)P(OEt)_3]^{3+}$ at pH 9.0 showed a more complicated pattern[17] than at pH 2.0, as a result of the mixture of at least three reaction products. One of the components was identified as a paramagnetic species,[18] which was also found in the mixture of photoreaction products after irradiation. Unfortunately, the identity of this species has not been unequivocally established. By analogy with the literature data,[17,18] *trans*-$[Ru(NH_3)_4(H_2O)P(OEt)_3]^{3+}$ may be assigned as a precursor of this paramagnetic species.

The results of our experiments strongly suggest that *trans*-$[Ru(NH_3)_4(H_2O)P(OEt)_3]^{2+}$ is the primary reaction product in the photochemistry of *trans*-$[Ru(NH_3)_4(NO_2)P(OEt)_3]^{2+}$. It is also stable unless a very reactive radical is present to trap this cation and initiate, probably through a chain reaction, its oxidation with a consequent decomposition through alterations

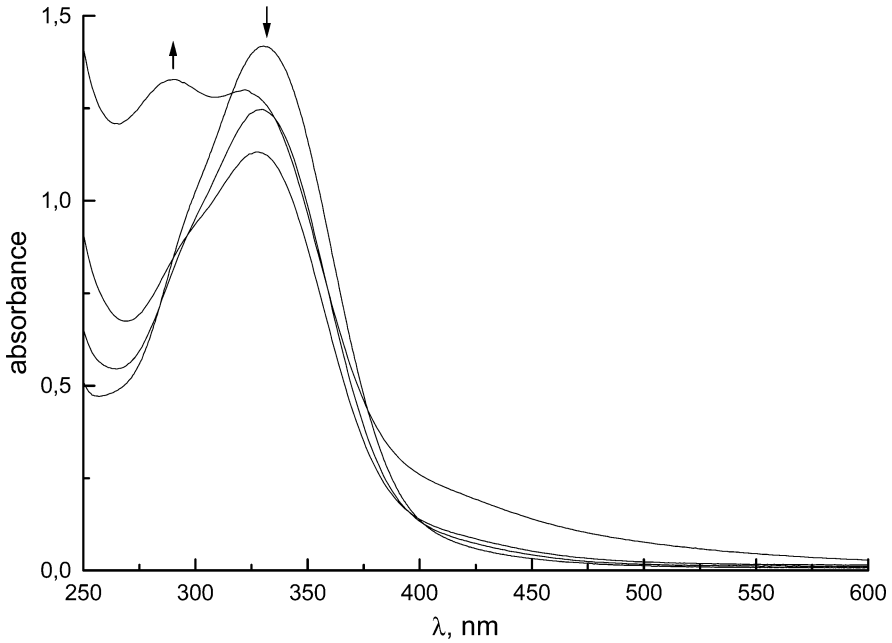

Figure 7. Spectral changes of the absorption spectrum accompanying the photolysis of *trans*-$[Ru(NH_3)_4(NO_2)P(OEt)_3]^+$ in phosphate buffer pH 9.3, $\lambda_{irr} =$ 355 nm.

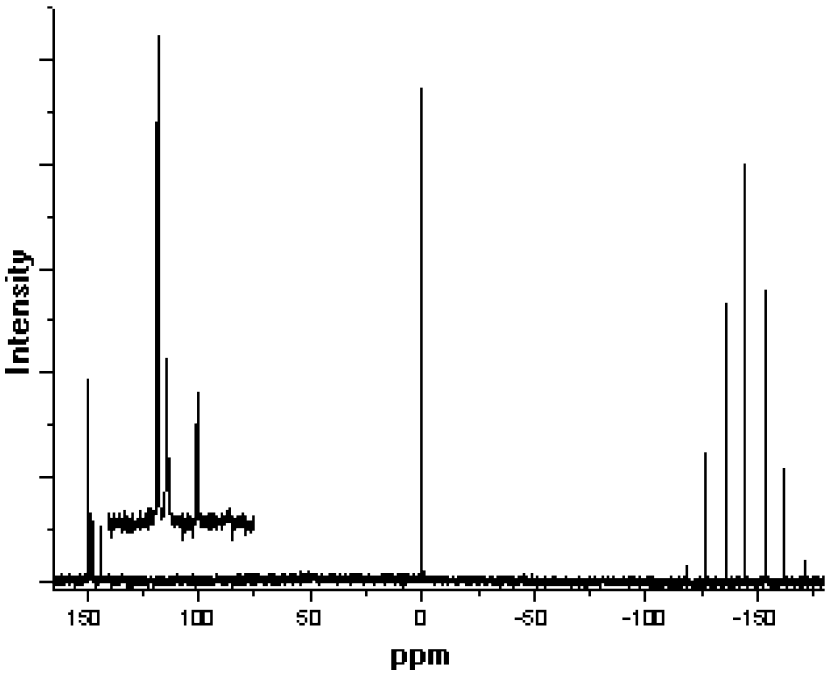

Figure 8. ^{31}P NMR spectrum of *trans*-$[Ru(NH_3)_4(NO_2)P(OEt)_3]^+$ in borax-buffered D_2O (pH 9.0) after 20 min of photolysis.

of the oxidized complex. The most obvious oxidant is a hydroxide radical, as it is produced during the photolysis of nitrite ion in alkaline solutions.[31]

To provide support for this hypothesis, ascorbic acid was introduced as a trap for any key intermediate produced during the photolysis of *trans*-$[Ru(NH_3)_4(NO_2)P(OEt)_3]^{2+}$. As is described in the literature,[34] the ascorbate anion, AH^-, would be oxidized by either $OH^\bullet$ or $NO_2^\bullet$ radical produced by the photolysis of nitrite in aqueous solution (Scheme 2).

In control experiments, nitrite (0.25 mol L^{-1}) was irradiated with 355 nm light in the presence of ascorbic acid (0.01 mol L^{-1}). There was an increase in the formation of the ascorbyl radical during irradiation, as is confirmed by in-situ EPR measurements. The EPR signals of the ascorbyl radical disappeared in the dark. On the contrary, the signals increased when the nitrite ion was replaced by the *trans*-$[Ru(NH_3)_4(NO_2)P(OEt)_3]^+$ complex.

The irradiation of *trans*-$[Ru(NH_3)_4(NO_2)P(OEt)_3]^+$ (0.028 mol L^{-1}) in the presence of ascorbic acid (0.057 mol L^{-1}) inside the EPR cavity resulted in a continuous decrease of the ascorbyl radical signal, as a function of time, Figure 10.

The ascorbyl radical acts as a trap for $OH^\bullet$, $NO_2^\bullet$, and $NO^\bullet$ and as a reductor for Ru(III), thereby preventing the generation of new species capable of initiating a chain reaction

(34) Bilski, P.; Chignell, C. F.; Szychlinski, J.; Borkowsky, A.; Olesky, E.; Reszka, K. *J. Am. Chem. Soc.* **1992**, *114*, 549−556.

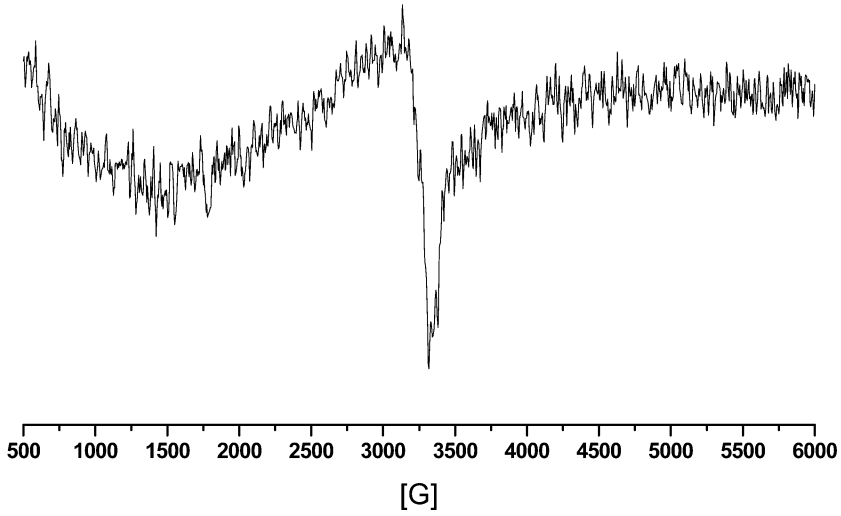

Figure 9. EPR spectrum of *trans*-[Ru(NH$_3$)$_4$(NO$_2$)P(OEt)$_3$]$^+$ complex in phosphate buffer pH 9.0 frozen after 20 min of irradiation at 355 nm.

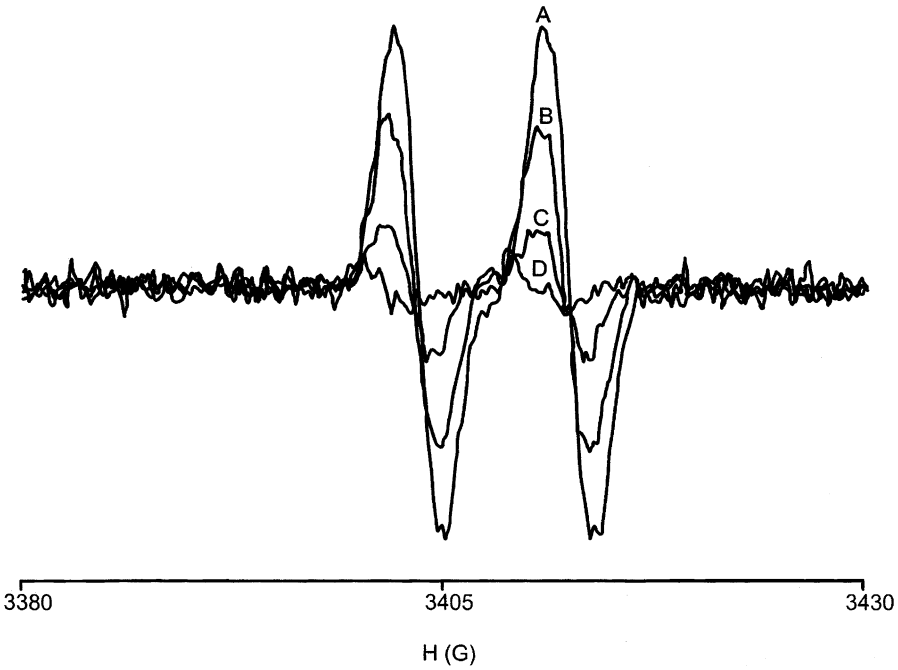

Figure 10. EPR spectrum of *trans*-[Ru(NH$_3$)$_4$(NO$_2$)P(OEt)$_3$]$^+$ complex in phosphate buffer pH 9.0 in the presence of ascorbic acid frozen after 20 min of irradiation at 355 nm. (A) Laser off, (B) laser on for 1 min, (C) laser on for 5 min, (D) laser on for 15 min.

Scheme 2. Reaction of the Radicals Produced during NO_2^- Photolysis in the Presence of Ascorbic Acid

$$NO_2^- \xrightarrow{h\nu} \{NO_2^-\}^*$$

$$\{NO_2^-\}^* \rightarrow NO^\bullet + O^{\bullet-}$$

$$OH^\bullet + NO_2^- \rightarrow NO_2^\bullet$$

$$O^{\bullet-} + H_2O \longrightarrow OH^\bullet + OH^-$$

$$AH^- + NO_2^\bullet \rightarrow A^{\bullet-} + HNO_2$$

$$AH^- + OH^\bullet \rightarrow A^{\bullet-} + H_2O$$

leading to the depletion of *trans*-[Ru(NH$_3$)$_4$(H$_2$O)P(OEt)$_3$]$^{2+}$. In addition, the recombination reaction of Ru(III) and AH$^-$ and/or A$^{\bullet-}$ as a termination step of a chain reaction would also be consistent with a decrease in the ascorbyl radical signals during the photolysis of *trans*-[Ru(NH$_3$)$_4$(NO$_2$)P(OEt)$_3$]$^{2+}$. From these results, it is evident that the rate for hydroxide abstraction by Ru(II) would be much faster than the rate for radical recombination[34] (OH$^\bullet$ + NO$_2^\bullet$ → HNO$_2$; $k = 1.0 \times 10^{10}$ L mol^{-1} s^{-1}).

The fact that *trans*-[Ru(NH$_3$)$_4$(H$_2$O)P(OEt)$_3$]$^{2+}$ is produced during the photolysis of *trans*-[Ru(NH$_3$)$_4$(NO$_2$)P(OEt)$_3$]$^+$ either in CH$_3$CN or in aqueous solution indicates that the principal deactivation pathway of the initial MLCT state is an internal conversion to a common reactive state, presumably the ^{3}LF* excited state to which ligand photolabilization is attributed. It is likely that the secondary photolysis of free nitrite occurs. In aqueous solution, this deactivation pathway leads to the formation of a hydroxide radical, which in the presence of *trans*-[Ru(NH$_3$)$_4$(H$_2$O)P(OEt)$_3$]$^{2+}$ would initiate a chain reaction. The observation of *trans*-[Ru(NH$_3$)$_4$(H$_2$O)P(OEt)$_3$]$^{3+}$ as a reaction product in aqueous solution suggests the following reaction sequence (Scheme 3).

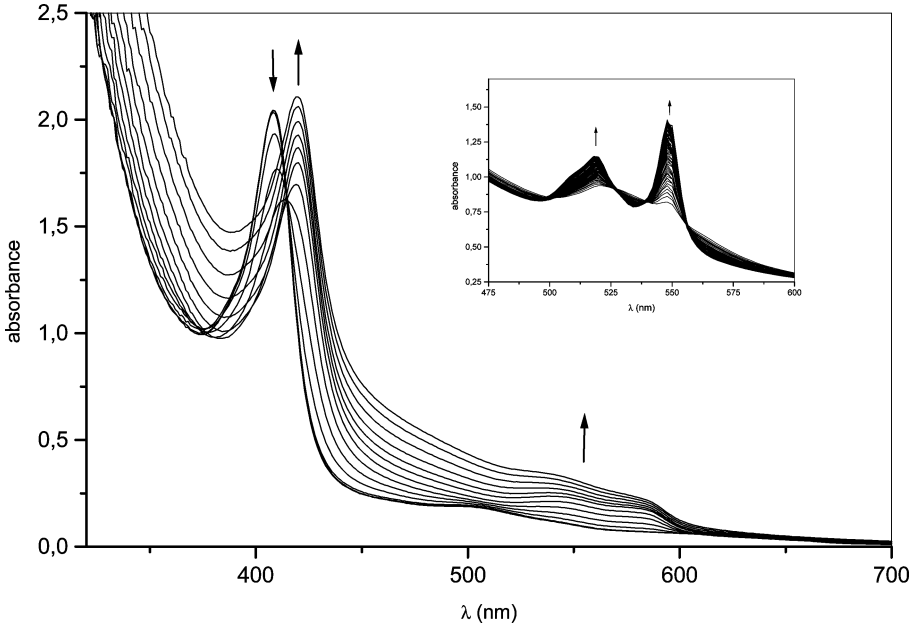

Figure 11. Spectral changes accompanying the formation of nitrosylmyoglobin (NO)Mb(II) from the thermal reaction of Mb(III) and *trans*-$[Ru(NH_3)_4(NO_2)P(OEt)_3]^+$ complex, after 15 min of photolysis, in phosphate buffer pH 7.4. Inset: Spectral changes observed for Cyt(III) during the thermal reaction with photolyzed *trans*-$[Ru(NH_3)_4(NO_2)P(OEt)_3]^+$ complex in phosphate buffer pH 7.4.

Scheme 3. Mechanism Proposed for the Reaction of *trans*-$[Ru(NH_3)_4(NO_2)P(OEt)_3]^+$ upon 355 nm Light Irradiation

$$trans\text{-}[Ru(NH_3)_4(NO_2)P(OEt)_3]^+ \xrightarrow{h\nu} trans\text{-}[Ru(NH_3)_4(H_2O)P(OEt)_3]^{2+} + NO_2^-$$

$$NO_2^- \xrightarrow{h\nu} NO^\bullet + O^{\bullet-}$$

$$O^{\bullet-} + H_2O \rightarrow OH^\bullet + OH^-$$

$$trans\text{-}[Ru(NH_3)_4(H_2O)P(OEt)_3]^{2+} + OH^\bullet \rightarrow trans\text{-}[Ru(NH_3)_4(H_2O)P(OEt)_3]^{3+} + OH^-$$

$$trans\text{-}[Ru(NH_3)_4(H_2O)P(OEt)_3]^{3+} \rightarrow Ru^{II}/Ru^{VI}$$

The presence of nitric oxide in this photoreaction is demonstrated by the experiments of heme proteins nitrosylation described below.

Reductive Nitrosylation. The direct reactions of NO with iron metalloproteins are the most important biological reactions in which NO participates.[3] For instance, the scavenging of NO by oxymyoglobin makes the heme protein a protector of cellular respiration through this function, where the otherwise slow oxidation of NO to nitrate is catalyzed efficiently.[35] NO also binds to iron in other heme proteins such as myoglobin, cytochromes, and hemoglobin.[3] In this context, attention has been devoted to the absorption spectroscopic studies on the interaction of heme proteins with NO generated from the photolyzed solution of *trans*-$[Ru(NH_3)_4(NO_2)P(OEt)_3]^+$. These studies are described below.

Myoglobin. The electronic spectrum of myoglobin, Mb(III), in phosphate buffer pH 7.4 exhibits absorption maxima at 408 nm ($\epsilon = 1.5 \times 10^5$ mol L^{-1} cm^{-1}) and 500 nm ($\epsilon = 1.0 \times 10^4$ mol L^{-1} cm^{-1}).[22] When the Mb(III) was mixed to the photolyzed solution of *trans*-$[Ru(NH_3)_4(NO_2)P(OEt)_3]^+$, Figure 11, new bands appeared at 418 nm in the Soret band region and at 536 and 567 nm in the Q-band region, because of the formation[22,23] of (NO)Mb(III). After a few minutes, the latter bands were red-shifted to 545 and 578 nm, while the one at 418 nm decreased to 420 nm. The overall spectral change was interpreted as the reductive nitrosylation of Mb(III), as the spectrum of (NO)-Mb(II) produced by the reaction of Mb(II) and NO also has absorption peaks[22] at 420 ($\epsilon = 1.29 \times 10^5$ mol L^{-1} cm^{-1}), 545, and 578 nm.

Hemoglobin. The absorption spectral changes of hemoglobin(III), $\lambda_{abs} = 403$ nm, in the presence of a photolyzed solution of *trans*-$[Ru(NH_3)_4(NO_2)P(OEt)_3]^+$ were studied in phosphate solutions. The NO adduct of hemoglobin, Hb(III), $\lambda_{abs} =$ 417 nm in the Soret band region and 532 and 563 nm in the Q-band region,[22] initially produced was gradually changed to (NO)Hb(II), 417, 542, and 570 nm. The mechanism involved in the formation of (NO)Hb(II) appears to be analogous to that of (NO)Mb(II) formation from Mb(III).

Cytochrome C. An anaerobic solution of *trans*-$[Ru(NH_3)_4(NO_2)P(OEt)_3]^+$, 0.006 g in 5 mL, was photolyzed with 355 nm light for 6 min. When the irradiation was stopped, cytochrome C, cyt(III), 0.002 g, was introduced into the cuvette. Notably, the spectrum measured over a period of minutes after the initiation of the reaction was identical to that of authentic reduced cytochrome C, cyt(II) (413, 518, and 549 nm).[22,23] The subsequent spectral changes which exhibit isosbestic points are interpreted in terms of (NO)cyt(II) formation.

Although preliminary, it is interesting to stress that, in our experiment, cytochrome C, which is structurally quite different from Mb(III) and Hb(III), reacts faster with photolyzed *trans*-$[Ru(NH_3)_4(NO_2)P(OEt)_3]^+$ than do Mb(III) and Hb(III).

Conclusions

The absorption spectrum of *trans*-$[Ru(NH_3)_4(NO_2)P(OEt)_3]^+$ is dominated by an intense MLCT transition band, but irradiation at 355 nm leads to photosubstitution processes typical of LF photochemistry. The irradiation wavelength of 355 nm is very close in energy to that of the lower energy ligand field band determined by TD-DFT calculations (406 nm), which are ascribed to a $d_{z2} \leftarrow d_{xz},d_{yz}$ transition. In the C_{4v} point group, the lowest LF states involve the population of σ^* states directed along the $O_2N-Ru-P(OEt)_3$ axis. The nitro labilization in the

(35) Moller, J. K. S.; Skibsted, L. H. *Chem. Rev.* **2002**, *102*, 1167−1178.

Ru(II) complex is consistent with the electron-withdrawing nature of this ligand, which leads to enhanced positive charge density in the nitro ligand, thus lowering its σ-donor capability relative to the phosphite ligand and leading to increased lability.

The photochemical behavior of *trans*-$[Ru(NH_3)_4(NO_2)P(OEt)_3]^+$ in the presence of hemeproteins in physiologic pH displays reactivity properties relevant to the mechanisms of NO reactions with Fe(III) proteins in vivo and proves that *trans*-$[Ru(NH_3)_4(NO_2)P(OEt)_3]^+$ is a potential photochemical delivery agent of NO to biological targets. Furthermore, the *trans*-$[Ru(NH_3)_4(H_2O)P(OEt)_3]^{2+}$ species produced would act as an antioxidant, as it is efficiently trapped by reactive hydroxyl radicals. It is important to note that as far as we know in vitro generation of a (NO)hem adduct from the photochemical activation of a metal transition complex has not been previously reported.

Acknowledgment. The authors would like to acknowledge FAPESP, CNPq, and CAPES for the grants and fellowships given to the research. They are also indebted to Prof. Bruce R. McGarvey for his helpful discussions and Prof. Peter C. Ford for reading and commenting on this manuscript.

Supporting Information Available: X-ray crystallographic data for structure determinations of *trans*-$[Ru(NH_3)_4(NO_2)P(OEt)_3]^+$ (CIF). This material is available free of charge via the Internet at http://pubs.acs.org.

JA0373263